

Article

Improved Electronic Transport in Ion Complexes of Crown Ether Based Columnar Liquid Crystals

Peter Staffeld ¹, Martin Kaller ², Philipp Ehni ², Max Ebert ², Sabine Laschat ^{2,*} and Frank Giesselmann ^{1,*} 

¹ Institut für Physikalische Chemie, Universität Stuttgart, Pfaffenwaldring 55, D-70569 Stuttgart, Germany; peter.staffeld@googlemail.com

² Institut für Organische Chemie, Universität Stuttgart, Pfaffenwaldring 55, D-70569 Stuttgart, Germany; m.kaller@icloud.com (M.K.); philipp.ehni@oc.uni-stuttgart.de (P.E.); max.ebert@oc.uni-stuttgart.de (M.E.)

* Correspondence: sabine.laschat@oc.uni-stuttgart.de (S.L.); f.giesselmann@ipc.uni-stuttgart.de (F.G.); Tel.: +49-711-68564565 (S.L.); +49-711-68564460 (F.G.)

Received: 21 December 2018; Accepted: 29 January 2019; Published: 31 January 2019



Abstract: The Li⁺- and K⁺-complexes of new discotic mesogens, where two n-alkoxy-substituted triphenylene cores are connected by a central crown ether (12-crown-4 and 18-crown-6), provide interesting structural and electronic properties. The inter- and intra-columnar structure was investigated by small and wide angle X-ray scattering. The electronic and ionic transports were studied by temperature dependent photoconductivity and impedance spectroscopy, respectively. Besides a strong increase of the stability and the width of the columnar phases the presence of soft anions (iodide, thiocyanate, tetrafluoroborate) leads to an improved intra-columnar order. The hereby shortened stacking-distance of the triphenylene cores leads to a significant increase of the photoconductivity in the columnar mesophase. Furthermore, the ionic conductivity of the new materials was investigated on macroscopically aligned thin films. The existence of channels for fast cation transport formed by the stacked crown ether moieties in the centre of each column can be excluded. The cations are coordinated strongly and therefore contributing only little to the conductivity. The ionic conductivity is dominated by the anisotropic migration of the non-coordinated anions through the liquid, like side chains favouring the propagation parallel to the columns. Iodide migrates about 20 times faster than thiocyanate and 100 times faster than tetrafluoroborate.

Keywords: liquid crystals; columnar; discotic; crown ether; electron transport; ion transport; ion channels; impedance spectroscopy; photoconductivity; X-ray diffraction; salt effect

1. Introduction

Columnar phases of discotic liquid crystals display one-dimensional (1D) photoconductivity according to a seminal discovery by Haarer et al. in 1993 [1], turning the investigation of the electronic charge transport in columnar liquid crystals into a very active field of research [2,3]. Columnar materials can be used as semiconductors in applications, like organic field effect transistors (OFET) [4,5], organic light emitting diodes (OLED) [6], or organic photovoltaic cells (OPV) [7]. The main advantage of using organic materials with liquid crystalline phases is the easy alignment, which facilitates the processing of the organic semiconductor significantly [5]. Currently, the design of discotic mesogens providing good charge transport properties in a suitable temperature range is of major interest [8–10]. Among these materials liquid crystalline crown ethers are particularly promising providing a unique entry into supramolecular chemistry due to their known propensity for selective metal salt complexation [11–13]. Previously, we reported about bi-centred liquid crystalline crown ethers and the impact of the molecular flexibility and geometry on structure and electronic charge transport properties in their columnar

phases [14]. The mesogens consisted of a central crown ether that connects two n-alkoxy substituted triphenylene cores [15,16]. We demonstrated that the structure and the electronic transport along the stacked triphenylenes are strongly affected by the above-mentioned molecular parameters. The mesogen carrying a small rigid 12-crown-4 connecting the two triphenylenes as symmetric as possible led to the formation of a broad mesophase with high intra-columnar order, which provided the highest hole mobility among the investigated compounds [14]. Furthermore, complexation of 12-crown-4 and 18-crown-6 with Li^+ and K^+ salts, respectively, carrying soft anions rather than hard halides resulted in significant broadening or even the induction of columnar mesophases [17]. Complementary ^1H and ^{13}C NMR experiments in solution [17,18] revealed that the use of soft polarizable anions, like iodide and thiocyanate, led to the formation of tight ion pairs in the case of the KI- and KSCN-complex of the 18-crown-6 derivative. These results suggested that Coulomb interactions between the mesogens should improve the columnar order.

Previously reported small angle X-ray diffraction data revealed that the broad columnar hexagonal phase ($p6mm$) of the neat 12-crown-4 derivatives became even wider after complexation with LiI and the lattice constant a increased [15]. On the other hand, the neat 18-crown-6 derivatives possessed a narrow columnar rectangular mesophase ($c2mm$) [18]. Due to the coordination of K^+ ions accompanied by soft anions the phase type changed. The KI and KBF_4 complexes displayed a highly ordered Col_r phase with $p2mg$ symmetry, while the KSCN complex showed a highly ordered Col_r phase with $p2gg$ symmetry.

Since the observed salt-induced changes in the phase behaviour must be related to the molecular arrangement of the columns, the stacking of the triphenylenes within the column should be affected as well. Thus, we surmised that ion uptake should not only change the structure, but also the electronic transport. This concept of combining aromatic groups for the electronic transport along the stacks with a crown ether that is able to coordinate specific types of cations leads to several possible features of the columnar phase. The coordination of ion pairs provides the unique opportunity to change the intra-columnar packing of the mesogens without varying any of the important remaining material parameters, like the aromatic cores or the lateral side chains (Figure 1).

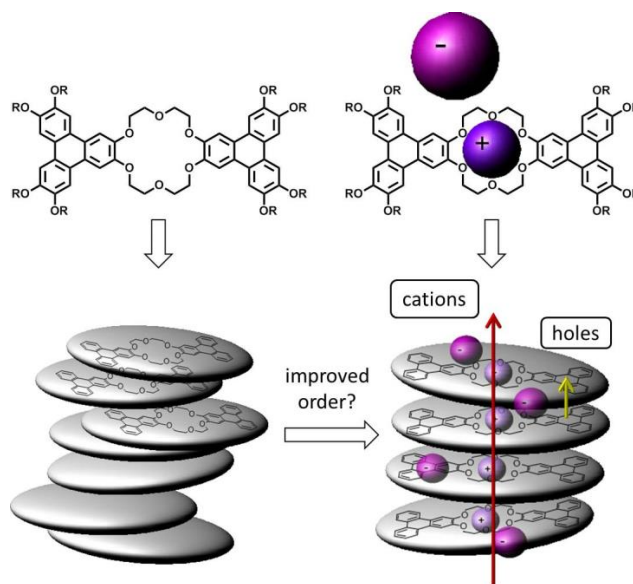


Figure 1. Structures of the bi-centred crown ether based discotic mesogens in this study and the expected impact of salt complexation. The coordinated ions are expected to improve the order and thus the hole transport via the stacked triphenylenes. Furthermore, the mesophase should provide channels for fast cation transport along the columns due to the stacked crown ether moieties.

Furthermore, we anticipated that, most likely, anisotropic ionic conductivity might be induced in the columnar phase. Since the crown ether moieties are stacked on top of each other in the centre of the columns channels for fast cation transport might be generated in the mesophase [19]. For smectic liquid crystal phases, strongly anisotropic two-dimensional (2D) ionic conductivity was demonstrated [20]. The transport of Li^+ in smectic phases of PEO-based (poly(ethylene)oxide) mesogens [21,22] is up to 100 times faster parallel to the smectic layers than perpendicular to them. Similar behavior was found for H^+ in smectic phases of mesogens with terminal diol-moieties [23]. Additionally, in columnar phases, strongly anisotropic 1D ion transport through the column centre was already observed by Yoshio et al. in columnar phases of an imidazolium-based ionic liquid crystal [24]. Beginn et al. could show that the membranes of polymerized columnar phases of liquid crystalline crown ethers where 4–5 molecules form supramolecular discs are at least permeable for several ions [25,26].

In the current study, the validity of the concept outlined in Figure 1 was probed by investigation of the electronic and ionic transport in the mesophase of the Li^+ -complex of 12-crown-4 and the K^+ -complex of 18-crown-6 based discotic mesogens. The transport properties were studied by photoconductivity (electronic transport) and impedance spectroscopy (ionic transport), respectively, and they were correlated to structural observations from X-ray experiments. As described below, our results reveal that the enhanced intra-columnar order in the KSCN and KI complexes of the 18-crown-6 derivative leads to improved photoconductivity, which is mainly due to anion mobility rather than cation transport.

2. Materials and Methods

2.1. Synthesis of the Crown Ether Salt Complexes

LiI complexes of 12-crown-4 **LiI-1a** ($\text{R} = \text{C}_9\text{H}_{19}$) and **LiI-1b** ($\text{R} = \text{C}_{12}\text{H}_{25}$) were prepared according to our previously published procedure [15]. KX complexes of 18-crown-6 **KI-2a** ($\text{R} = \text{C}_9\text{H}_{19}$) and **KI-2b**, **KSCN-2b** ($\text{R} = \text{C}_{11}\text{H}_{23}$), and **KI-2c**, **KSCN-2c**, and **KBF₄-2c** ($\text{R} = \text{C}_{12}\text{H}_{25}$) were prepared according to our previously reported method [18]. The complexation of the known crown ethers **1a,b** and **2a–c** was performed by adding a solution of the crown ether in CH_2Cl_2 to a solution of 1.5 equiv. of the respective LiI or KX salt in MeOH, stirring for 18 h at room temperature, followed by filtration, and then evaporation of the solvent. As described in refs. [16–18], the formation of (1:1) complexes was monitored by the characteristic ^1H and ^{13}C NMR chemical shifts and MALDI-TOF MS spectra.

2.2. X-Ray Diffraction

Small angle X-ray scattering experiments were performed on a SAXSess system (Anton Paar, Graz, Austria), equipped with an advanced collimation block providing a very narrow line shaped X-ray beam. The X-ray source is a Cu-K_α X-ray tube providing a monochromatic wavelength of 0.1542 nm. The detector is either a CCD camera with a pixel size of $24 \times 24 \mu\text{m}^2$ or a $5 \times 20 \text{ cm}$ imaging plate read out in a imaging plate reader (Perkin Elmer Cyclone plus, Waltham, MA, USA). The sample is contained in quartz capillaries, with a diameter of 0.7 mm being placed in a temperature controlled sample holder (25–300 °C). The accessible q-range is $0.04\text{--}27 \text{ nm}^{-1}$.

The wide angle X-ray scattering experiments have been performed on a home-made imaging plate camera with a sample to imaging plate distance of 10 cm. The source is a Cu-K_α X-ray tube (Siemens Kristalloflex X-ray generator, Erlangen, Germany), providing a monochromatic wavelength of 0.1542 nm. The sample is placed in a small hole (about 2 mm in diameter) in a brass block as thin film and was kept between two permanent magnets providing a magnetic field of about 2 Tesla. The imaging plate is developed in an imaging plate reader (Fujifilm BAS SR, Tokyo, Japan). A Lakeshore 331 controller varies temperature.

To avoid the precipitations of the salt the compounds were filled into the capillary or the hole as a powder. During the X-ray experiments, the samples were never heated above their clearing point.

2.3. Photoconductivity

The sample was contained in typical liquid crystal glass cells (0.8 and 1.3 μm gap) equipped with ITO (Indium Tin Oxide) electrodes and rubbed polyimide alignment layers on both sides. Cells were filled with the isotropic melt of the compounds by capillary action. The temperature of the sample was controlled by a hot stage (Mettler Toledo FP-5, Columbus, OH, USA). A dc electric field of $0.25\text{--}1\text{ V } \mu\text{m}^{-1}$ is applied by a power supply. The sample was illuminated by a Xe-lamp (Perkin Elmer 150 W, Waltham, MA, USA) at a certain wavelength that was adjusted by an optical filter at (366 ± 5) nm or a monochromator (Horiba Spex 1681B, Kyoto, Japan). The light was chopped at the frequency of 6 Hz by a mechanical chopper, while a lock-in amplifier detected the photocurrent (Stanford Research Systems SR830 DSP, Sunnyvale, CA, USA). Data acquisition was done by a computer equipped with *LabView*.

2.4. UV/Vis Spectroscopy

Spectra were taken using a UV-Vis Spectrometer (Perkin Elmer Lambda 2, Waltham, MA, USA) with a wavelength range of 190–1100 nm. The samples are contained in 0.8 μm polyimide coated liquid crystal cells that were placed in a homemade temperature controlled sample holder.

2.5. Alignment and Polarizing Microscopy

The alignment of the sample and the changes in texture at the phase transitions have been tracked by a polarizing microscope (Olympus BH-2, Tokyo, Japan) equipped with a hot stage (Instec Mk2, Boulder, CO, USA). Large homeotropic aligned domains could be grown in parallel rubbed polyimide coated cells after careful thermal cycling close to the clearing point. All of the compounds showed a certain degree of macroscopic segregation between complex and neat compound after heating to the isotropic melt.

2.6. Impedance Spectroscopy

An impedance analyser (Hewlett Packard 4192 A, 5 Hz–13 MHz, Palo Alto, CA, USA), equipped with a homemade temperature controller was used. The amplitude of the ac-voltage was set to 0.2 V. The sample was measured using interdigitating platinum electrodes ($d = 225$ nm) on glass substrates (Schott AF45, Jena, Germany). The electrode structure provided a channel length of 5 μm and a total width of 115 μm . The ac-response of a liquid crystalline sample on interdigitating electrodes can be modelled by a simple RQ-equivalent circuit (Figure 2). Q is a constant phase element accounting for the slightly depressed semicircles in the *Nyquist* diagram.

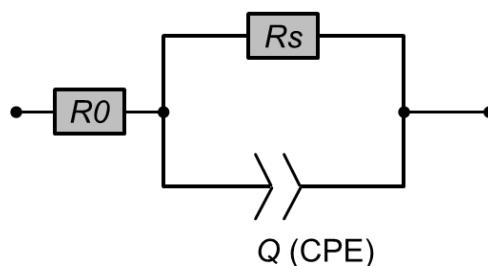


Figure 2. Equivalent circuit for the modeling of the impedance measurements. R_0 is the resistance of the wires and the electrodes themselves. R_s is the bulk dc-resistance of the sample and Q is the constant phase element (CPE).

The bulk resistance R_s was deduced from the diameter of the semicircle in the *Nyquist* diagram. The cell constant A in cm^{-1} was determined by calibrating the setup with 1 mM KCl-solution of known conductivity. The ionic dc-conductivity σ_{ion} was determined according to:

$$\sigma_{ion} = \frac{A}{R_s} \quad (1)$$

The liquid crystal was put on the surface covered by a thin glass slide and then heated to the columnar phase to equilibrate. The specific alignment of the columns was achieved by shearing the material in the liquid crystal phase either parallel or perpendicular to the electric field of the interdigitating electrodes. Data analysis was done using *ZView* (Scribner Associates Inc., Southern Pines, NC, USA).

3. Results and Discussion

3.1. Mesophase Structure of the Complexes

Figure 3 shows the investigated liquid crystalline crown ethers. The well-defined cavity size of the crown is responsible for the coordination of specific types of cations, which leads to the formation of (1:1) complexes with several ion pairs in solution.

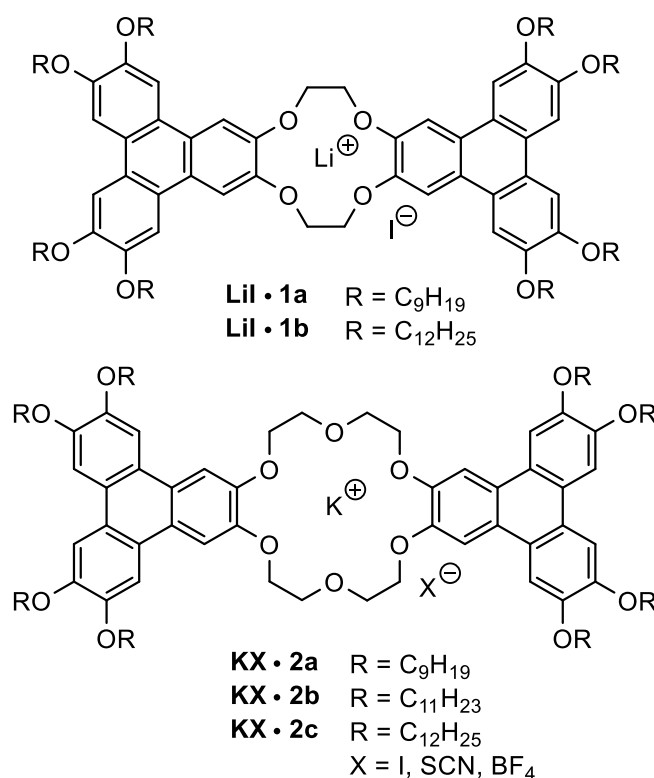


Figure 3. Investigated LiI-complexes of the 12-crown-4 and KX-complexes (X = I, SCN, BF₄) of the 18-crown-6 derivative bearing lateral side chains of OC₉H₁₉, OC₁₁H₂₃, and OC₁₂H₂₅.

For the detailed determination of the mesophase structure and the analysis of the electronic and ionic transport properties the alignment of the materials is of crucial importance. After filling the isotropic melt of the complexes into polyimide coated liquid crystal cells, it turned out that a significant part of the coordinated salt was macroscopically precipitated. The conglomerate was visible in the light microscope. This led to a phase separation of the free crown ether and the complex. Figure 4 shows the polarizing micrographs of the columnar phase of **KSCN-2b** in a liquid crystal cell after cooling down from the isotropic melt. Above 132 °C, dark parts are visible that are due to isotropic neat crown ether **2b** (Figure 4a). Upon further cooling (top to bottom) the isotropic-to-columnar phase transition of neat **2b** at 132 °C was clearly visible (Figure 4b).

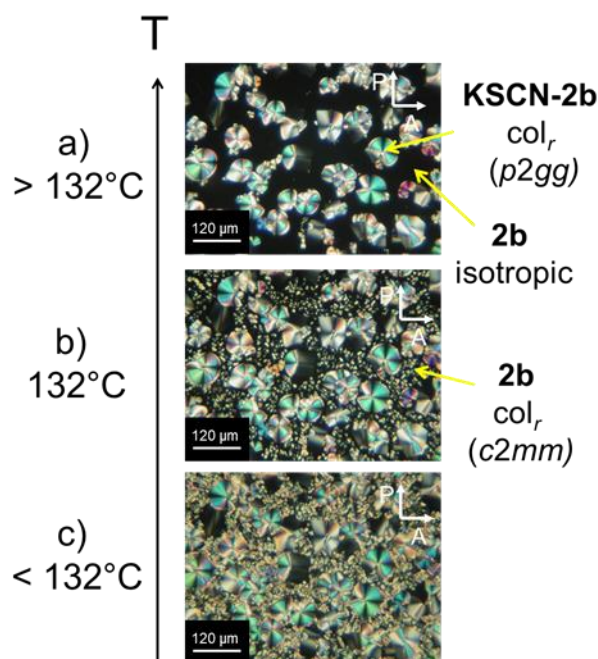


Figure 4. KSCN-2b sample in a polyimide coated cell after cooling down from the isotropic melt. Above 132 °C (a) the macroscopic segregation of the complex (texture) and isotropic free crown **2b** (dark parts) can be seen clearly. By cooling down (top to bottom) the isotropic-columnar phase transition (b) of **2b** at 132 °C can be observed. In (c), the columnar phase of KSCN-2b and neat **2b** coexist.

Approximately half of the crown ether complexes in the sample kept their ion pairs and they were able to self-assemble into the columnar mesophase even after repetitive heating/cooling cycles. For the 18-crown-6 derived K^+ complexes the tendency towards thermal decomplexation was dependent on the counterions. Complexes with SCN^- were more stable than those with I^- , BF_4^- , Br^- , and Cl^- counterions. In case of Cl^- or Br^- , the respective salt KCl or KBr precipitated already partially in the columnar phase and completely after heating to the isotropic phase. Due to the problems that are caused by the thermal decomplexation, we focused on the 18-crown-6 complexes **KI-2b** and **KSCN-2b** and the corresponding 12-crown-4 complex **LiI-1b** and re-examined them by SAXS (small-angle X-ray scattering).

The known diffraction patterns for **KI-2b** (Col_r , $p2mg$), **LiI-1b** (Col_h , $p6mm$), and **KSCN-2b** (Col_r , $p2gg$) [15–18] could be confirmed. However, for **KSCN-2b**, we discovered an additional 46 K wide high temperature phase with $p2mg$ symmetry between 190 °C and the clearing point at 236 °C (Figure 5, Table S1). The lattice constants of the low temperature phase ($p2gg$) $a = 53.1$ Å and $b = 47.4$ Å (at 180 °C) are very similar to those found previously [15–18]. The lattice parameters of the new high temperature phase ($p2mg$) $a = 64.1$ Å and $b = 38.2$ Å (at 220 °C) are significantly different. Figure 5 shows the small angle diffraction patterns of both columnar phases and the solid state of a polydomain sample of **KSCN-2b**. The X-ray data with the respective Miller indices are summarized in Table S1. In both columnar phases, numerous sharp reflexes can be observed, indicating a high degree of inter-columnar order.

In the solid state of **KSCN-2b**, instead the diffraction pattern changed to diffuse scattering, where only one single broad peak plus a small shoulder could be clearly identified. At higher angles, several broad peaks were detected, indicating that the well-defined crystal structure of neat **2b** (see [14]) is turned into a glassy state g by the coordination of KSCN. The SAXS pattern in Figure 5 however indicates, that the inter-columnar order of the $p2gg$ phase is not fully preserved in the glassy state, which might originate from conformational changes of the mesogens below the glass transition. The new phase sequence of **KSCN-2b** is shown in Figure 6. Since the Col_r - Col_r phase transition could neither

be seen via POM (polarizing optical microscopy) or DSC (differential scanning calorimetry) on cooling, the value is shown in parentheses.

Even though we do not have the full XRD data set for complex **KSCN-2c** due to lack of material, we assume that the phase behaviour is rather similar to **KSCN-2b**, since both of the complexes showed very similar behaviour in the DSC (Figure S2 in the Supplementary Materials) as well as in the POM.

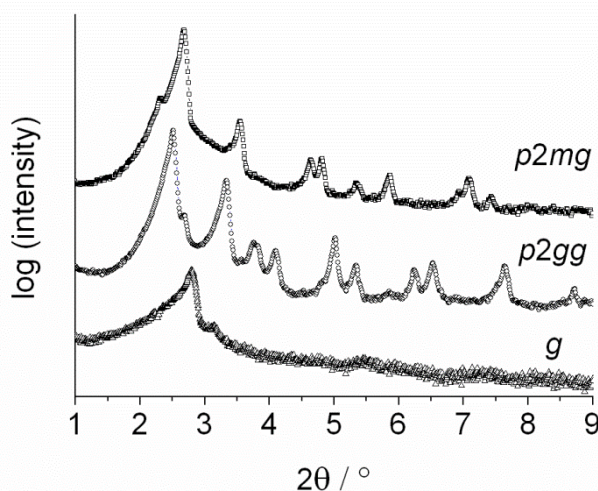


Figure 5. Small angle diffraction pattern of the new high temperature Col_r -phase ($p2mg$) (\square) at 220 °C, the already known col_r -phase ($p2gg$) (\circ) at 180 °C and the solid state (g) at 20 °C (Δ) of **KSCN-2b**.

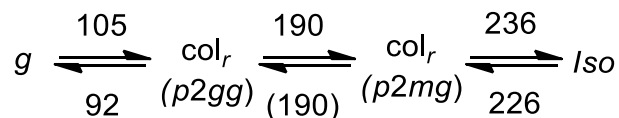


Figure 6. New phase sequence of **KSCN-2b**. The phase sequence of **KSCN-2c** is assumed to be very similar.

After having clarified the mesophase geometries, we wondered how the coordination of ions might affect the intra-columnar order and thus the electronic properties of the material. Therefore, we performed detailed wide angle X-ray diffraction experiments. Figure 7 exemplarily shows the comparison of the wide angle diffraction patterns of neat crown ethers **1b**, **2c**, and their respective LiI- and KSCN-complexes.

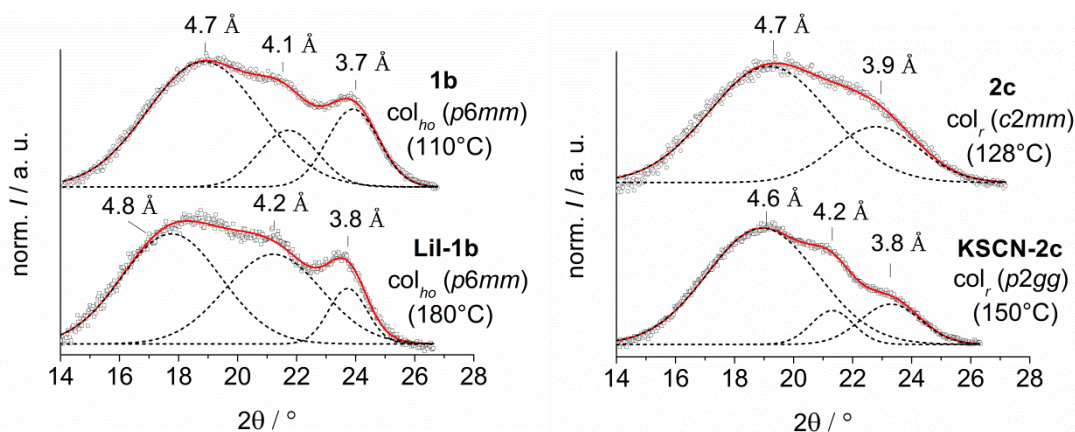


Figure 7. Wide angle diffraction patterns of **1b** vs. **LiI-1b** (left) and **2c** vs. **KSCN-2c** (right). An additional peak can be observed in the diffraction pattern of **KSCN-2c** due to the ion coordination. The dotted curves divide the scattering pattern in single Gaussian distribution functions.

The XRD patterns of the 12-crown-4 derivatives **1b** and **LiI-1b** were very similar. In each case, three peaks could be observed. The broad halo at lowest angle is attributed to the liquid, like alkyl chains with a mean distance of about 4.7 Å. The peak at highest angle belongs to the stacking of the triphenylene cores with a mean distance of 3.7 Å. The peak in the middle is probably due to the periodic arrangement of the small rigid crown ethers. The distance between the crown ether units is about 4.1–4.2 Å. The scattering of the triphenylenes indicated a slightly increased correlation length (lower peak width) in the case of **LiI-1b** as compared to **1b**.

The XRD patterns of the 18-crown-6 derivatives showed clear differences. While the scattering of the crown ether units cannot be observed in neat **2c** the peak was visible in the complex **KSCN-2c**. Furthermore, the stacking period of the triphenylenes decreased from 3.9 to 3.8 Å. Presumably, due to the coordination of K^+ , the flexibility of the crown ether is restricted by the coordinative bonds of the oxygen atoms to the central cation.

This model is in good agreement with previous studies on crystal structures of salt complexes of aryl-substituted crown ethers, which revealed that oxygen atoms are arranged in a plane surrounding the cation and the aromatic residues are oriented out of this plane, leading to a bowl-shaped arrangement [27–30]. Such planar arrangement should result in decreased intracolumnar distances between neighboring mesogens. The increased order of the oxygen atoms leads to the additional diffraction peak at 4.2 Å, which was observed only for the small rigid 12-crown-4 derivatives **1**.

These results show that the coordination of ions promotes a higher intra-columnar order. The strong broadening of the columnar phases can be explained by these findings. The increased order and the decreased stacking distance of the triphenylenes should improve the electronic transport along the stacks.

In the solid state the complexes **LiI-1b** and **KSCN-2c** showed the expected broad diffraction patterns bearing only diffuse peaks (Figure S4), which are typical for a glassy state. Since the intra-columnar order is very low, the electronic charge transport should be disfavoured in the solid states of the complexes.

3.2. Electronic Transport

The combination of photoconductivity measurements and impedance spectroscopy allows for the complementary detection of either the electronic or the ionic transport in the columnar material. The use of these two different methods provides insight into the electronic properties of mixed conductors. We chose the lock-in technique to measure the photoconductivity, because it is a useful tool to separate the electronic from the ionic transport. For a good charge transport along the stacked triphenylene columns, homeotropic alignment in the liquid crystal cell is required. The alignment was achieved by surface interaction of the mesogens at the isotropic-to-columnar phase transition. For the subsequent experiments, **KSCN-2c** was used, because it showed sufficient stability during repetitive heating/cooling cycles and the growth of large homeotropically aligned domains of the complex on the electrode area. According to our previous results, neither the crown ether size nor the length of the side chains influences the absorbance spectra of the compounds [14]. In current experiments, we observed that the presence of coordinated salts in the crown does not change the shape and position of the absorption bands as exemplified for **2b** and **KSCN-2b** (Figure S2). Since the liquid crystal cells are fabricated from glass blocking wavelengths shorter than 310 nm, the only suitable optical transitions are the absorption bands at 346 and 363 nm belonging to the vibration fine structure of the $S_0 \rightarrow S_1$ transition of the triphenylene unit [31].

Figure 8 shows the typical temperature dependent photoconductivity profile of **KSCN-2c** (red curve) without any contributions from the segregated **2c** due to its edge-on (planar) alignment. The measurement was obtained using a 3.5 µm polyimide coated cell that was illuminated at 370 nm via monochromator. The applied electric field was held at 1 V µm⁻¹. The second graph shows the photoconductivity profile of neat **2c** (black curve). The photoconductivity of **KSCN-2c** displayed a strong dependence on the phase type and temperature. As expected, in the isotropic state, the

photocurrent is very close to zero. Both Col_r mesophases ($p2mg$ and $p2gg$) instead provided significant photoconductivity. The maximum response was detected at about $160\text{ }^\circ\text{C}$ in the low temperature mesophase with $p2gg$ symmetry. The glassy solid state g appears to be completely insulating regarding the electronic transport. All of the phase transitions were visible in the profile, but they are not as distinct as in the corresponding photoconductivity profile of the neat crown ether **2c**, making the assignment of a sharp transition temperature difficult. The highest signal for the neat crown ether **2c** was measured in the crystalline states Cr_1 , Cr_2 at about $65\text{ }^\circ\text{C}$, while the rectangular columnar phase ($c2mm$) between 123 and $133\text{ }^\circ\text{C}$ showed considerably lower photoconductivity. All of the phase transitions were very distinct in the profile of neat **2c**. It is evident from Figure 9 that neat 18-crown-6 **2c** and the complex **KSCN-2c** display complementary behaviour. The electronic transport in the crystalline solid state of **2c** was totally suppressed by ion uptake. In contrast, in the columnar phase of neat 18-crown-6 **2c**, no electronic transport was detected, whereas ion uptake, i.e., the formation of the complex **KSCN-2c** resulted in a significant increase of the electronic transport as compared to the glassy solid state.

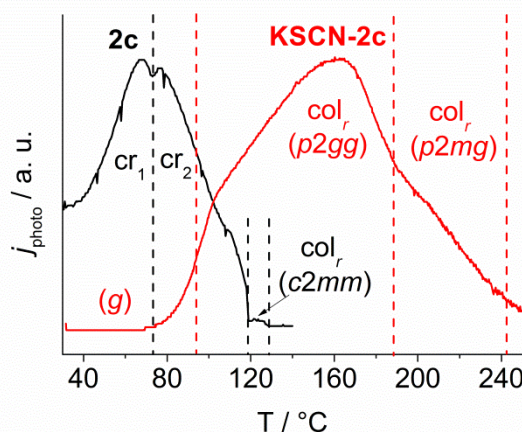


Figure 8. Typical normalized temperature dependent photoconductivity profile of **KSCN-2c** (red) and neat **2c** (black). The phase transitions are depicted by the color coded vertical dashed lines for **2c** and **KSCN-2c**. Neat **2c** shows low photocurrent in the columnar phase ($c2mm$) and a significantly raised signal in both crystalline solid states Cr_1 and Cr_2 . The complex instead shows an “inverted” profile. The two columnar phases ($p2gg$ and $p2mg$) provide significant photoconductivity while the signal vanishes completely in the glassy solid g . In both cases, no current could be detected in the isotropic melt.

To achieve optimum conditions for quantitative comparison of the photoconductivity in the columnar phases of both compounds, neat 18-crown-6 **2c** and **KSCN-2c** were aligned in a $0.8\text{ }\mu\text{m}$ polyimide-coated cell. The applied electric field was held at $0.25\text{ V }\mu\text{m}^{-1}$ and both light intensity and wavelength were controlled by an optical filter at $(366 \pm 5)\text{ nm}$. The measurement was performed between the clearing point of the respective compound and room temperature at a cooling rate of 2 K min^{-1} . Figure 9a) shows the comparison of the measured photocurrent j_{photo} in the Col_r phases of neat **2c** and **KSCN-2c**. The homeotropic alignment of neat **2c** and **KSCN-2c**, respectively, on the electrode area in the cell are shown in Figure 9b,c.

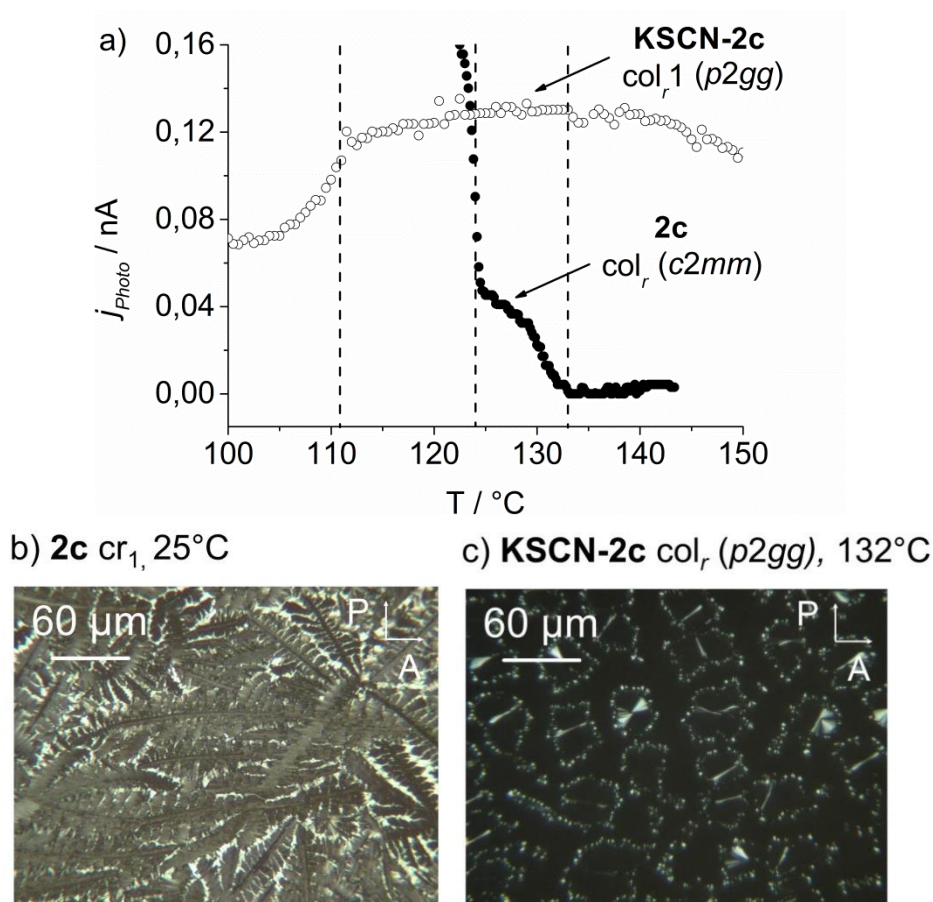


Figure 9. Temperature dependent photoconductivity (a) of the columnar phase of neat **2c** (●) and the low temperature columnar phase of **KSCN-2c** (○) both contained in a 0.8 μm LC (liquid crystal) cell. The polarizing micrographs show the nearly homeotropically aligned neat **2c** (b) all over the electrode area, in contrast to the phase separated **KSCN-2c** in the liquid crystal cell (c).

It should be emphasized that a quantification of the experimentally determined photocurrents has to be considered with great care for several reasons. Only about 50% of the electrode area in the **KSCN-2c** sample was covered with the homeotropically aligned mesophase of the complex, while the remaining area was partly covered with free 18-crown-6 derivative **2c**, which is isotropic at temperatures exceeding 120 $^{\circ}\text{C}$ and thus does not contribute to the total photoconductivity. In the sample of neat **2c**, about 90% of the electrode area was covered (Figure 9). This means that the effective intersection of the light beam with the photoactive parts of **KSCN-2c** is only about half as large as it is in the sample of neat **2c**. Additionally, a weakening of the internal dc-field in **KSCN-2c** due to the formation of electrolytic double-layers at the electrode surface in the presence of ions should be expected. This is not the case for neat **2c**. Despite these limitations, the results in Figure 10 suggest that the photoconductivity in the columnar phase of **KSCN-2c** is about three times higher as compared to the neat 18-crown-6 **2c**, which is in agreement with the changes of the inter- and intracolumnar structure, as determined by SAXS and WAXS (wide-angle X-ray scattering) experiments. Unfortunately, the exact determination of the charge carrier mobility with the organic field effect transistor (OFET) was not possible for the complexes. The desired field effect current was strongly superimposed by the ionic current flow.

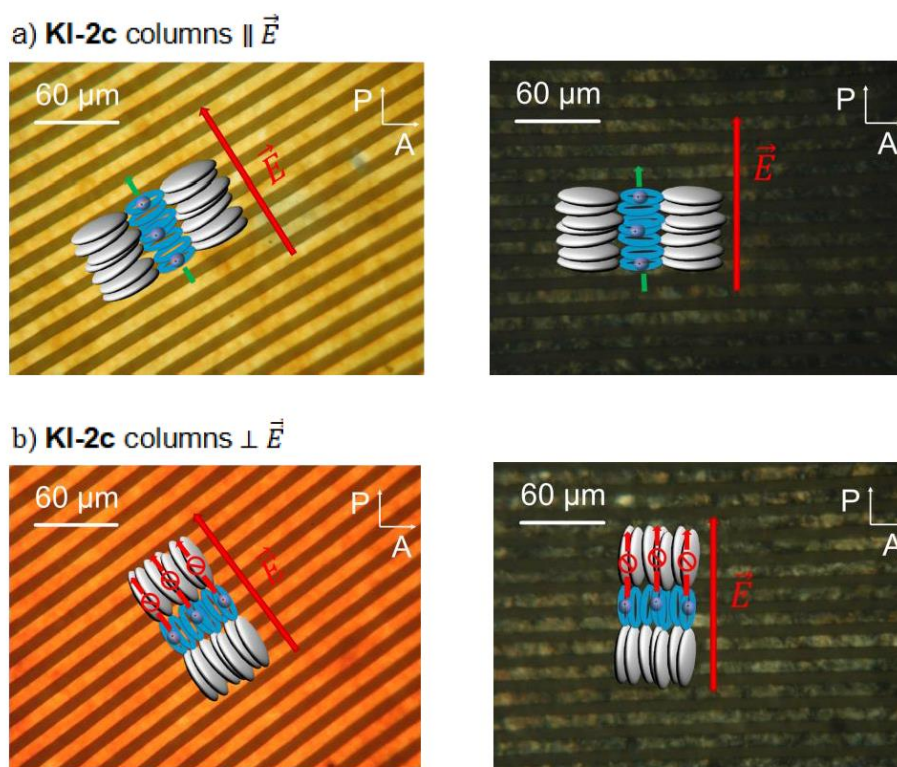


Figure 10. Bright and dark state polarizing micrographs of KI-2c films on interdigitating electrodes with columns aligned parallel to the electric field direction (a) and columns aligned perpendicular to the electric field direction (b).

3.3. Ionic Transport

To investigate the ionic conductivity, we performed impedance spectroscopy, which is a powerful tool to measure the bulk ionic dc-conductivity. Since the use of liquid crystal cells for these measurements was impossible due to the precipitation of the coordinated salt we used interdigitating gold electrodes. The liquid crystalline material was held at temperatures that were only slightly above the melting point during sample preparation.

In order to clarify, whether coordinated cations in the centre of each mesogen could migrate through the stacked crown ether moieties as 1D transport channels, experiments were carried out on planar aligned films with columns either parallel or perpendicular to the electric field direction. Figure 10 shows two aligned films of KI-2c in the liquid crystal phase at 140 °C in the bright and dark state between crossed polarizers. Since the photographs have been taken in reflexion, the bright stripes in the bright states are the platinum electrodes. In Figure 10a, the columns of the LC phase are aligned parallel to the electric field, while in Figure 10b the columns are aligned perpendicular.

By comparing the interference colour of the films in linear polarized light with samples of known thickness in liquid crystal cells, the thickness of the films could be estimated to be about 5 μm. Van Gerwen et al. calculated the electric field distribution in the case of interdigitating electrodes [32]. Applying this method to our geometry, where the 230 nm high and 5 μm wide electrode digits are separated by 5 μm, a minimum film thickness of 10 μm is required to cover 100% of the electric stray field. On the other hand, a 5 μm thick film still covers about 80% and the thickness of both films is quite similar (yellow/orange main colour). This means that the comparison of the measured dc-conductivity values for the films should be reliable.

Figure 11 shows the results for KI-2c measured parallel to the columns at 150 °C in the LC-phase. The frequency dependence of the total impedance $|Z|(\omega)$ and the phase angle $\phi(\omega)$ are displayed in

the *Bode* diagram. Furthermore, the *Nyquist* diagram $-Z''$ (Z') is shown where the imaginary part of the impedance is plotted versus the real part, leading to a semicircle.

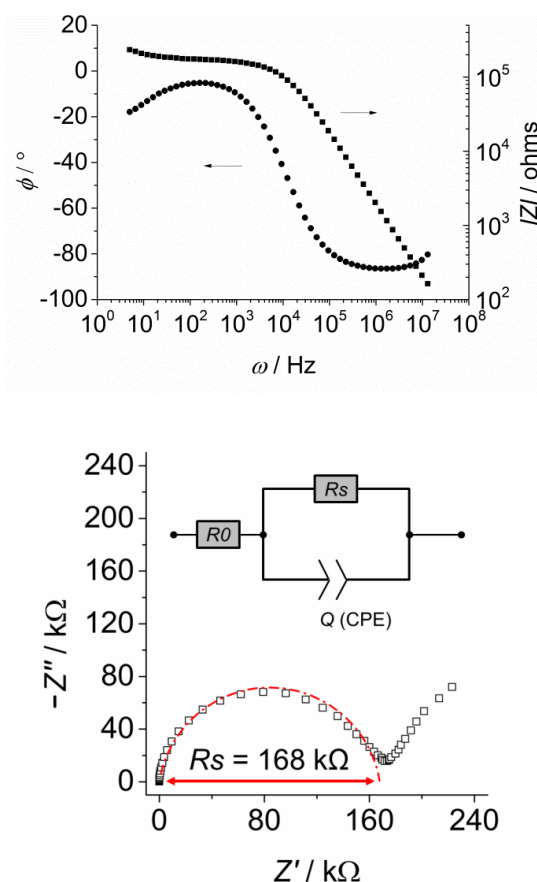


Figure 11. *Bode* plot showing the frequency dependence of the total impedance $|Z|(\omega)$ and the phase angle $\phi(\omega)$ (top) and the *Nyquist* plot $-Z''$ (Z') (imaginary part vs. real part of the impedance) showing a slightly depressed semicircle that was fitted by the equivalent circuit shown in the inset (bottom).

The equivalent circuit we used for fitting the data is shown in the inset. The pre-resistance of the wires and the platinum electrodes themselves is represented by R_0 . It is in series with the standard RQ-circuit that was used for the modelling of electrolytes on interdigitating electrode structures. The constant phase element Q accounts for the slightly depressed shape of the semicircle. The diameter of the semicircle is given by the bulk dc-resistance R_s of the film. With the specific cell constant A of 0.0076 cm^{-1} , the ionic dc-conductivity is determined from Equation (2) (see below). At low frequencies, the onset of a second semicircle could be observed in the *Nyquist* diagram. This phenomenon could be due to the formation of an ionic double layer at the electrode surface. Another possibility would be the contribution of a second transport process, for example, the migration through domain boundaries. In crystalline solids, the strong effect of grain boundaries on the charge transport is well known [33]. Since the low frequency arc did not affect the measurement results, its origin was not investigated further. Figure 12 shows the ionic conductivity parallel σ_{\parallel} and perpendicular σ_{\perp} to the columns determined from the measurements of the aligned films of **KI-2c** shown in Figure 10. Both of the films were measured between 120 and 155 °C in the Col_r phase ($p2gg$).

It is clearly seen that σ_{\parallel} is slightly higher than σ_{\perp} , but the maximum anisotropy at 155 °C ($= 2.33 \times 10^{-3}/\text{K}$ in Figure 12) is only $\sigma_{\parallel}/\sigma_{\perp} = 1.7$. If channels for fast K^+ transport exist in the columnar phase, the value of σ_{\parallel} should be much higher than σ_{\perp} . Parallel to the columns, the cations should migrate through the stacked crown ethers but perpendicular to the columns the cations cannot contribute to the conductivity, since they would have to leave their coordination site (compare the inset of Figure 10).

In comparison to liquid crystalline materials providing channels for fast ion transport with anisotropy values between 10 and 100 [21,23,24], the observed difference in conductivity is most probable not due to the 1D transport of the coordinated K^+ cations. Furthermore, the measured conductivity values turned out to be rather low never exceeding $10^{-7} \text{ S cm}^{-1}$, which is not typical for materials featuring ion channels. The measured anisotropy was in the order of magnitude of a conventional nematic liquid crystal where the anisotropy in ionic conductivity is just caused by the anisotropic structure of the liquid crystal, as shown by Stegemeyer et al. [34]. Presumably, the K^+ ions are strongly coordinated and the ion migration should be dominated by the non-coordinated anions that migrate through the side chains of the columnar system. Since the transport seems not to be dependent on the orientation of the columns in the liquid crystal phase and other investigated compounds showed anisotropy values ≤ 1.7 , the following measurements were carried out on randomly aligned thicker films ($>10 \mu\text{m}$).

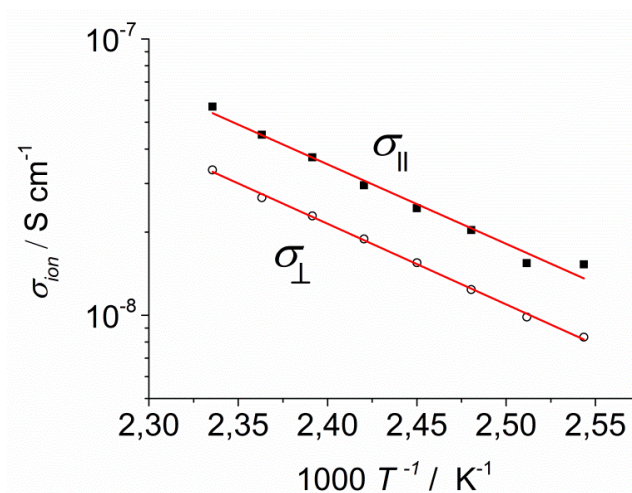


Figure 12. Arrhenius diagram of the ionic conductivity parallel σ_{\parallel} (■) and perpendicular σ_{\perp} (○) to the columns in the columnar phase of **KI-2c**.

Since the anion seems to play the decisive role, we investigated the K^+ complexes **KX-2c** with different anions ($X = \text{I, SCN and BF}_4$) (Figure 13). Upon using smaller counter ions, like Br^- or Cl^- , the precipitation of the respective salt already took place at the solid-to-columnar phase transition, making it impossible to get reproducible conductivity values.

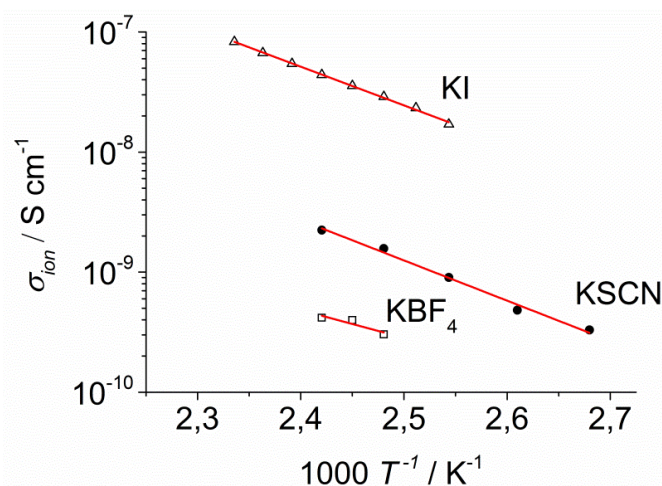


Figure 13. Arrhenius diagram of the ionic conductivity of **KI-2c** (Δ), **KSCN-2c** (\bullet), and **KBF₄-2c** (\square).

The conductivity for **KI-2c** ($4 \times 10^{-8} \text{ S cm}^{-1}$ at $140 \text{ }^\circ\text{C} = 2.42 \times 10^{-3}/\text{K}$ in Figure 13) was 20 times higher than for **KSCN-2c** and 100 times higher than for **KBF₄-2c**. This result suggests that the anions dominate the contribution to the ionic conductivity. This result might be rationalized by SCN^- acting as a bridging ligand. If the SCN^- is coordinating two K^+ complexes, then it would be firmly incorporated in the columnar structure, which would be detrimental to its mobility in the electric field. On the contrary, the less polarizable BF_4^- might be less soluble in the liquid crystal and precipitation of KBF_4 might cause a lower charge carrier concentration and thus lower conductivity.

Thus, different kinds of counter ions have a strong impact on the ionic conductivity of the columnar phase. Since the melting points were in the same temperature range ($125 \text{ }^\circ\text{C}$ for **KI-2c**, **KBF₄-2c** and $110 \text{ }^\circ\text{C}$ for **KSCN-2c**) and all of the compounds form columnar rectangular mesophases, a similar viscosity was proposed for these derivatives. Among the tested anions, I^- is traveling much faster than SCN^- or BF_4^- , resulting in more than one order of magnitude higher conductivity. These results indicate comparatively strong bound cations in the centre of the crown ether moiety of each mesogen plus mobile anions that are located mainly in the peripheral liquid, like side chains. The observed anisotropy of $\sigma_{\parallel}/\sigma_{\perp} = 1.7$ (at $155 \text{ }^\circ\text{C}$) could be explained by considering the local viscosity anisotropy of the side chains, since the viscosity scales with the order parameter of the alkyl chains. This might indicate enhanced conductivity perpendicular to the columns, which was not observed. On the other hand, ions migrating along the columns do not have to overcome the barriers of stacked crown ether moieties. Thus, ion migration along the columns might be favorable for the anions.

Since the anions seem to be mobile parallel and perpendicular to the columns (Figure 12), we assume that they are located mainly in the amorphous side chains of the columnar system. The viscosity η of the solvent influences the ion mobility μ_{ion} , according to the Stokes–Einstein equation:

$$\mu_{ion} = \frac{ze}{6\pi\eta r_{ion}} \quad (2)$$

where z describes the charge number, e the elementary charge, and r_{ion} the radius of the solvated ion. By the variation of the side chains it should be possible to change the environment of the anions specifically, since the cations are located in the centre of the columns. By elongation of the side chains, the local viscosity should be lowered, which would result in higher ion mobility according to Equation (2). A similar effect is expected by enlarging the central crown ether moiety. Therefore, we compared thick films ($>10 \mu\text{m}$) of the iodide-complexes with different chain lengths ($-\text{OC}_9\text{H}_{19}$ or $-\text{OC}_{12}\text{H}_{25}$), namely **LiI-1a,b** and **KI-2a,c** (Figure 14).

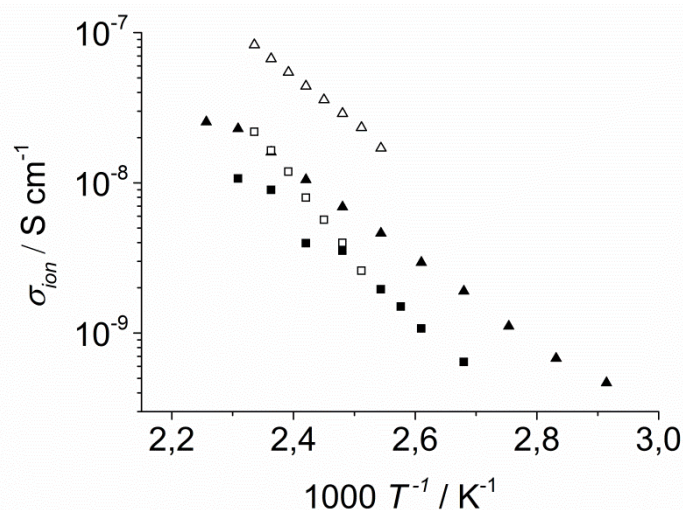


Figure 14. Arrhenius diagram of the ionic conductivity of **LiI-1a** (■), **LiI-1b** (▲), **KI-2a** (□), and **KI-2c** (△). Both pairs of compounds with neat and filled symbols, respectively, bear the same ion pairs but they differ in side chain length.

Upon comparison of the homologues with different side chain length, the derivatives with C12 chains (\blacktriangle and \triangle) showed higher conductivity than those with C9 chains (\blacksquare and \square). When comparing the K^+ complexes of the 18-crown-6 derivatives with the Li^+ complexes of the 12-crown-4 derivatives with identical side chains (\triangle vs. \blacktriangle and \square vs. \blacksquare) the higher conductivity was observed for the complexes **KI-2a,b**. The ion mobility can be increased by elongated side chains. Since the side chains should not affect the transport of the coordinated cations in the column centres, the results in Figure 14 suggest that the anions dominate the conductivity of the columnar phase and that they are located mainly in the amorphous side chains.

The observed anisotropy of $\sigma_{\parallel}/\sigma_{\perp} = 1.7$ favors the migration of the anions parallel to the columns. This might be rationalized by comparing these columnar systems with a nematic liquid crystal. In a conventional nematic liquid crystal, the transport of ions is favored parallel to the director, i.e., parallel to the long axis of the rod-like molecules. A value of the anisotropy $\sigma_{\parallel}/\sigma_{\perp} = 1.3$ was published by Stegemeyer et al. [34], which is somehow comparable to our case, if the columns of the columnar phases of the crown ether complexes are considered as rods of an ordered nematic phase.

When considering that only the anion contributes to the charge transport and that every mesogen incorporates one ion pair, it is also possible to derive mobility values for the different anions. The specific conductivity of electrolytes σ is given by:

$$\sigma = \Lambda_m c, \quad (3)$$

with Λ_m being the molar conductivity and c the concentration of charge carriers. Excluding the migration of cations, the molar conductivity can be calculated as:

$$\Lambda_m = |z_-|v_- F \mu_-, \quad (4)$$

where $|z_-|v_-$ is the electrovalence of the anions being 1 in our case, F is the Faraday-constant, and μ_- is the mobility of the anions. Since there is one anion per mesogen, the concentration can be estimated by the density of mesogens per unit volume in the columnar phase. Finally, the mobility of the anions can be derived from:

$$\mu_- = \frac{\sigma M}{F \varrho}, \quad (5)$$

with M as molar mass of the mesogen and ϱ the density of the phase.

While the density could not be experimentally measured, the crystallographic density of the crown ethers substituted with aromatic units was taken from the literature 1.3 g cm^{-3} [27–30]. The coordination of ions increases the density, while the substitution with long alkyl tails in turn decreases it. Therefore, the density of 1.3 g cm^{-3} should be appropriate. According to these estimations, the mobility of the anions was determined at $140 \text{ }^\circ\text{C}$ for the different compounds and they are summarized in Table 1. When comparing these values with the recently determined hole mobility of the Col_r phase of the neat **2c** [14], it can be seen that the hole transport in our materials is about four orders of magnitude faster than the anion transport.

Table 1. Calculated anion mobility in the columnar rectangular mesophases of **KI-2c**, **KSCN-2c**, and **KBF₄-2c** at $140 \text{ }^\circ\text{C}$ for the estimated density of 1.3 g cm^{-3} .

	Structure of the Phase	σ [S cm ⁻¹]	M [g mol ⁻¹]	μ_{anion} [cm ² V ⁻¹ s ⁻¹]
KI-2c	col _r (p2mg)	2.0×10^{-8}	2301.3	3.6×10^{-10}
KSCN-2c	col _r (p2gg)	2.2×10^{-9}	2232.5	4.0×10^{-11}
KBF₄-2c	col _r (p2mg)	4.2×10^{-10}	2261.2	7.5×10^{-12}

4. Conclusions

The ion complexes of different bi-centred liquid crystalline crown ethers that are based on 18-crown-6 and 12-crown-4 moieties were studied regarding a correlation between the structure of the mesophases and their electronic and ionic transport properties. XRD experiments revealed that the free 12-crown-4 **1b** and its complex **LiI-1b** both exhibit a broad columnar hexagonal mesophase. No significant differences were found regarding the intra-columnar order. In contrast, the free 18-crown-6 **2c** exhibited a columnar rectangular mesophase ($\Delta T = 13$ K) with $c2mm$ symmetry. Upon coordination of K^+ salts with soft anions, like I^- or SCN^- , the mesophase range was highly broadened and the symmetry of the phases changed. **KI-2c** possessed a Col_r phase ($\Delta T = 80$ K) with $p2mg$ symmetry. **KSCN-2c** displayed a high temperature Col_r phase ($\Delta T = 46$ K) with $p2mg$ symmetry and a low temperature Col_r phase ($\Delta T = 85$ K) with $p2gg$ symmetry.

Furthermore, **KSCN-2c** showed an improved intra-columnar order, leading to a better packing of the crown ether moieties plus a shortened stacking distance of the triphenylene cores of 3.8 Å in contrast to 3.9 Å for the neat compound **2c**.

The increased intra-columnar order had a pronounced impact on the photoconductivity where the detected signal was about three times higher in the columnar phase of **KSCN-2c** than in neat **2c**.

Investigation of the ion migration on macroscopically aligned thin films of **KI-2c** revealed that the dc-conductivity parallel to the columns in the liquid crystal phase was only slightly higher than perpendicular to them. The anisotropy was determined to be $\sigma_{||}/\sigma_{\perp} = 1.7$ for **KI-2c** at 155 °C. The type of the anion (I^- , SCN^- , BF_4^-) had a strong impact on the conductivity of the K^+ -complex of **2c**. **KI-2c** showed 20 times higher conductivity than **KSCN-2b** and conductivity that was 100 times higher than **KBF₄-2c**. From the dependence of the ionic conductivity on the size of the central crown and the length of the lateral side chains in **LiI-1a,b** and **KI-2a,b**, we concluded that the ion migration is dominated by the non-coordinated anions propagating through the anisotropic liquid, like side chains, while the cations are strongly bound in the centre of the columns. Thus, the existence of channels for fast cation transport could be excluded. It should be noted that Bardaj, Espinet, and coworkers recently reported similar ionic conductivities for K^+ complexes of diaza-18-crown-6 ethers carrying six decyloxy-p-cyanobiphenyl chains and showing nematic mesophases [35]. The corresponding Li^+ complexes showed 10 times higher conductivity, which was rationalized by cations that were jumping from one crown to another close to it [35].

As showcased for 18-crown-6 **2c** and the corresponding complexes **KX-2c** with different anions, the ion complexes form highly ordered columnar mesophases with improved stacking of the triphenylene cores, leading to increased 1D photoconductivity (Figure 15). The coordinated cations are strongly bound to the centre of the columns while the non-coordinated anions are mobile in the anisotropic liquid like side chains. The calculated mobility for **KX-2c** with different anions was in the order of 10^{-12} – 10^{-10} $cm^2 V^{-1} s^{-1}$, which is four orders of magnitude lower than the hole mobility of the neat 18-crown-6 **2c**. This again correlates well with the results by Bardaj, Espinet, and coworkers, which observed 20 times higher conductivity, when the crown ether metal complex was doped with the neat “empty” crown [35].

In conclusion, the complexation of columnar liquid-crystalline crown ethers did not lead to fast ion migration, as might be expected by the presence of crown ether channels. On the other hand, however, the coordination of ions in the channels improved the intra-columnar packing of the crown ether rings and thereby enhanced the electronic charge transport, namely the hole mobility. Even without fast ion channels, the complexation of liquid-crystalline crown ethers turned out to be a promising tool for tailoring the charge transport properties in this class of materials.

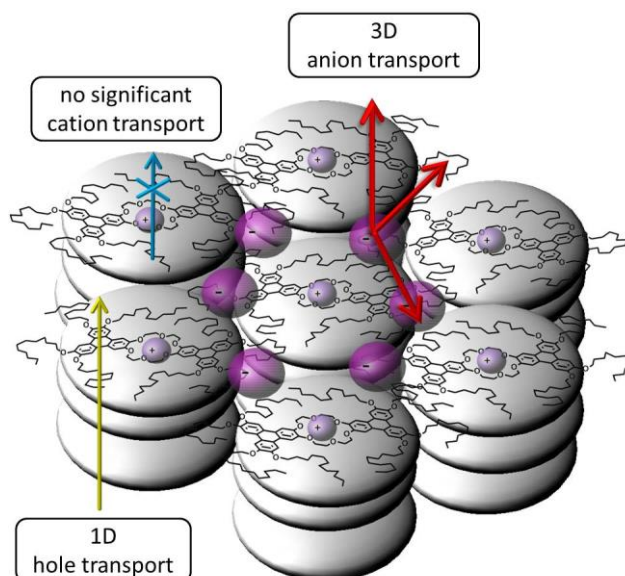


Figure 15. Our new mesogenic bi-centred ion complexes form highly ordered columnar mesophases providing improved quasi one-dimensional (1D) hole transport. The cations are coordinated strongly by the central crown ether moieties showing no significant contribution to the ionic conductivity. The anions are mobile in the anisotropic liquid like side chains.

Supplementary Materials: The following are available online at <http://www.mdpi.com/2073-4352/9/2/74/s1>. Figure S1: **KI-2b** in the columnar state ($p2mg$) (left) and in the solid state g (right). The texture shows no significant differences. Figure S2: DSC curves of the complexes **KSCN-2b** (a) and **KSCN-2c** (b). Heating/cooling rate 10 K/min. Figure S3: WAXS pattern of **KSCN-2b** taken from ref. [1]. Figure S4: Wide angle diffraction pattern of **LiI-1b** (○) and **KSCN-2c** (□) in the solid state. Only diffuse smeared peaks can be observed indicating a low intra-columnar order. Figure S5: Absorbance spectrum of neat **2b** (■) and its KSCN-complex **KSCN-2b** (●) in the solid state. Figure S6: Photoconductivity profiles of a segregated sample of **KSCN-2b** (Δ) where both components contribute to the photocurrent in the respective temperature ranges. Furthermore, the profile of neat **2b** (●) and a **KSCN-2b** sample (○) where only the complex contributes are shown. Figure S7: Large scale pictures of the aligned thin films of **KI-2b** between crossed polarizers in the bright state (left) and the dark state (right). The columns have been aligned parallel (A, B) and perpendicular (C, D) to the electric field. Figure S8: Temperature dependent ionic conductivity in thick films of **KI-2b** with columns aligned randomly (□), parallel (●) and perpendicular (▲) to the electric field. Table S1: Small angle X-ray data of **KSCN-2b**. θ is the scattering angle, hk the Miller indices, d_{ob} and d_{cal} are the observed and calculated distances while a and b are the lattice constants for the rectangular unit cell. Table S2: XRD data of **KSCN-2b** taken from ref. [1].

Author Contributions: Conceptualization, F.G. and S.L.; methodology, P.S. and M.K.; validation, P.S., M.K., F.G., S.L.; formal analysis, P.S., F.G., P.E., M.E.; investigation and synthesis, P.S., M.K.; data curation, P.S., F.G., S.L., P.E., M.E.; writing—original draft preparation, P.S., F.G., S.L.; writing—review and editing, S.L., P.E., M.E., F.G.; supervision, F.G., S.L.; project administration, F.G., S.L.; funding acquisition, F.G., S.L.

Funding: Generous financial support by the International Max Planck Research School for Advanced Materials (fellowships for P.S. and M.K.), the Deutsche Forschungsgemeinschaft (LA 907/17-1 SNAPSTER), the Bundesministerium für Bildung und Forschung (joint instrumentation grant) and the Ministerium für Wissenschaft, Forschung und Kunst des Landes Baden-Württemberg is gratefully acknowledged.

Conflicts of Interest: The authors declare no conflict of interest. The funders had no role in the design of the study; in the collection, analyses, or interpretation of data; in the writing of the manuscript, or in the decision to publish the results.

References

- Adam, D.; Closs, F.; Frey, T.; Funhoff, D.; Haarer, D.; Schuhmacher, P.; Siemensmeyer, K. Transient photoconductivity in a discotic liquid crystal. *Phys. Rev. Lett.* **1993**, *70*, 457–460. [[CrossRef](#)] [[PubMed](#)]
- Pisula, W.; Müllen, K. Discotic Liquid Crystals as Organic Semiconductors. In *Handbook of Liquid Crystals*, 2nd ed.; Goodby, J.W.G., Collings, P.J., Kato, T., Tschierske, C., Gleeson, H.F., Raynes, E.P., Eds.; Wiley-VCH: Weinheim, Germany, 2014; Volume 8, pp. 617–674.

3. Sergeev, S.; Pisula, W.; Geerts, Y.H. Discotic liquid crystals: A new generation of organic semiconductors. *Chem. Soc. Rev.* **2007**, *36*, 1902–1929. [[CrossRef](#)] [[PubMed](#)]
4. Pisula, W.; Zorn, M.; Chang, J.Y.; Müllen, K.; Zentel, R. Liquid crystalline ordering and charge transport in semiconducting materials. *Macromol. Rapid Commun.* **2009**, *30*, 1179–1202. [[CrossRef](#)] [[PubMed](#)]
5. Pisula, W.; Menon, A.; Stepputat, M.; Lieberwirth, I.; Kolb, U.; Tracz, A.; Siringhaus, H.; Pakula, T.; Müllen, K. A Zone-Casting Technique for Device Fabrication of Field-Effect Transistors Based on Discotic Hexa-*peri*-hexabenzocoronene. *Adv. Mater.* **2005**, *17*, 684–689. [[CrossRef](#)]
6. Seguy, I.; Destruel, P.; Bock, H. An all-columnar bilayer light-emitting diode. *Synth. Met.* **2000**, *111*–*112*, 15–18. [[CrossRef](#)]
7. Tang, C.W. Two-layer organic photovoltaic cell. *Appl. Phys. Lett.* **1986**, *48*, 183–185. [[CrossRef](#)]
8. Wöhrle, T.; Wurzbach, I.; Kirres, J.; Kostidou, A.; Kapernaum, N.; Litterscheidt, J.; Haenle, J.C.; Staffeld, P.; Baro, A.; Giesselmann, F.; et al. Discotic Liquid Crystals. *Chem. Rev.* **2016**, *116*, 1139–1241. [[CrossRef](#)]
9. Laschat, S.; Baro, A.; Steinke, N.; Giesselmann, F.; Hägele, C.; Scalia, G.; Judele, R.; Kapatsina, E.; Sauer, S.; Schreivogel, A.; et al. Discotic liquid crystals: From tailor-made synthesis to plastic electronics. *Angew. Chem. Int. Ed.* **2007**, *46*, 4832–4887. [[CrossRef](#)]
10. Eichhorn, H. Mesomorphic phthalocyanines, tetraazaporphyrins, porphyrins and triphenylenes as charge-transporting materials. *J. Porphyrins Phthalocyanines* **2000**, *4*, 88–102. [[CrossRef](#)]
11. Laschat, S.; Baro, A.; Wöhrle, T.; Kirres, J. Playing with nanosegregation in discotic crown ethers: From molecular design to OFETs, nanofibers and luminescent materials. *Liq. Cryst. Today* **2016**, *25*, 48–60. [[CrossRef](#)]
12. Kaller, M.; Baro, A.; Laschat, S. Liquid Crystalline Crown Ethers and Related Compounds. In *Handbook of Liquid Crystals*, 2nd ed.; Goodby, J.W.G., Collings, P.J., Kato, T., Tschierske, C., Gleeson, H.F., Raynes, E.P., Eds.; Wiley-VCH: Weinheim, Germany, 2014; Volume 6, pp. 335–376.
13. Kaller, M.; Laschat, S. Liquid crystalline crown ethers. *Top. Curr. Chem.* **2012**, *318*, 109–192. [[PubMed](#)]
14. Staffeld, P.; Kaller, M.; Beardsworth, S.J.; Tremel, K.; Ludwigs, S.; Laschat, S.; Giesselmann, F. Design of conductive crown ether based columnar liquid crystals: Impact of molecular flexibility and geometry. *J. Mater. Chem. C* **2013**, *1*, 892–901. [[CrossRef](#)]
15. Kaller, M.; Staffeld, P.; Haug, R.; Frey, W.; Giesselmann, F.; Laschat, S. Substituted crown ethers as central units in discotic liquid crystals: Effects of crown size and cation uptake. *Liq. Cryst.* **2011**, *38*, 531–553. [[CrossRef](#)]
16. Kaller, M.; Beardsworth, S.J.; Staffeld, P.; Tussetschläger, S.; Giebelmann, F.; Laschat, S. Increased mesophase range in liquid crystalline crown ethers via lower molecular symmetry. *Liq. Cryst.* **2012**, *39*, 607–618. [[CrossRef](#)]
17. Kaller, M.; Tussetschläger, S.; Fischer, P.; Deck, C.; Baro, A.; Giesselmann, F.; Laschat, S. Columnar mesophases controlled by counterions in potassium complexes of dibenzo-18crown-6 derivatives. *Chem. Eur. J.* **2009**, *15*, 9530–9542. [[CrossRef](#)] [[PubMed](#)]
18. Kaller, M.; Deck, C.; Meister, A.; Hause, G.; Baro, A.; Laschat, S. Counterion effects on the columnar mesophases of triphenylene-substituted 18crown-6 ethers: Is flatter better? *Chem. Eur. J.* **2010**, *16*, 6326–6337. [[CrossRef](#)]
19. Yoshio, M.; Kato, T. Liquid Crystals as Ion Conductors. In *Handbook of Liquid Crystals, Second Completely Revised and Greatly Enlarged Edition*; Goodby, J.W.G., Collings, P.J., Kato, T., Tschierske, C., Gleeson, H.F., Raynes, E.P., Eds.; Wiley-VCH: Weinheim, Germany, 2014; Volume 8, pp. 727–750.
20. Funahashi, M.; Yasuda, T.; Kato, T. Liquid Crystalline Semiconductors: Oligothiophene and Related Materials. In *Handbook of Liquid Crystals*, 2nd ed.; Goodby, J.W.G., Collings, P.J., Kato, T., Tschierske, C., Gleeson, H.F., Raynes, E.P., Eds.; Wiley-VCH: Weinheim, Germany, 2014; Volume 8, pp. 675–708.
21. Hoshino, K.; Kanie, K.; Ohtake, T.; Mukai, T.; Yoshizawa, M.; Ujiie, S.; Ohno, H.; Kato, T. Ion-conductive liquid crystals: Formation of stable smectic semi-bilayers by the introduction of perfluoroalkyl moieties. *Macromol. Chem. Phys.* **2002**, *203*, 1547–1555. [[CrossRef](#)]
22. Funahashi, M.; Shimura, H.; Yoshio, M.; Kato, T. Functional Liquid-Crystalline Polymers for Ionic and Electronic Conduction. In *Liquid Crystalline Functional Assemblies and Their Supramolecular Structures (Structure and Bonding)*; Kato, T., Bara, J.E., Eds.; Springer: Berlin, Germany, 2008; Volume 128, pp. 151–179.
23. Germer, R.; Giesselmann, F.; Zugenmaier, P.; Tschierske, C. Anomalous Electric Conductivity in Amphiphilic Smectic Liquid Crystals with Terminal Diol-Groups. *Mol. Cryst. Liq. Cryst.* **1999**, *331*, 643–650. [[CrossRef](#)]

24. Yoshio, M.; Mukai, T.; Ohno, H.; Kato, T. One-dimensional ion transport in self-organized columnar ionic liquids. *J. Am. Chem. Soc.* **2004**, *126*, 994–995. [[CrossRef](#)]
25. Beginn, U.; Zipp, G.; Möller, M. Functional Membranes Containing Ion-Selective Matrix-Fixed Supramolecular Channels. *Adv. Mater.* **2000**, *12*, 510–513. [[CrossRef](#)]
26. Beginn, U.; Zipp, G.; Mourran, A.; Walther, P.; Möller, M. Membranes Containing Oriented Supramolecular Transport Channels. *Adv. Mater.* **2000**, *12*, 513–516. [[CrossRef](#)]
27. Charland, J.P.; Buchanan, G.W.; Kirby, R.A. Reinvestigation of the structure of dibenzo-12-crown-4 ether. *Acta Crystallogr. C Cryst. Struct. Commun.* **1989**, *45*, 165–167. [[CrossRef](#)]
28. Buchanan, G.W.; Kirby, R.A.; Charland, J.P.; Ratcliffe, C.I. 12-Crown-4 ethers: Solid-state stereochemical features of dibenzo-12-crown-4, derived dicyclohexano-12-crown-4 isomers, and a lithium thiocyanate complex as determined via carbon-13 CPMAS nuclear magnetic resonance and x-ray crystallographic methods. *J. Org. Chem.* **1991**, *56*, 203–212. [[CrossRef](#)]
29. Buchanan, G.W.; Mathias, S.; Lear, Y.; Bensimon, C. Dibenzo-15-crown-5 ether and its sodium thiocyanate complex. X-ray crystallographic and NMR studies in the solid phase and in solution. *Can. J. Chem.* **1991**, *69*, 404–414. [[CrossRef](#)]
30. Blake, A.J.; Gould, R.O.; Parsons, S.; Radek, C.; Schröder, M. Potassium Dibenzo-18-crown-6 Triiodide. *Acta Crystallogr. C Cryst. Struct. Commun.* **1996**, *52*, 24–27. [[CrossRef](#)]
31. Markovitsi, D.; Germain, A.; Millie, P.; Lecuyer, P.; Gallos, L.; Argyrakos, P.; Bengs, H.; Ringsdorf, H. Triphenylene Columnar Liquid Crystals: Excited States and Energy Transfer. *J. Phys. Chem.* **1995**, *99*, 1005–1017. [[CrossRef](#)]
32. van Gerwen, P.; Laureyn, W.; Laureys, W.; Huyberechts, G.; de Beeck, M.O.; Baert, K.; Suls, J.; Sansen, W.; Jacobs, P.; Hermans, L.; et al. Nanoscaled interdigitated electrode arrays for biochemical sensors. *Sens. Actuators B* **1998**, *49*, 73–80. [[CrossRef](#)]
33. Rodewald, S.; Fleig, J.; Maier, J. Microcontact Impedance Spectroscopy at Single Grain Boundaries in Fe-Doped SrTiO₃ Polycrystals. *J. Am. Ceram. Soc.* **2001**, *84*, 521–530. [[CrossRef](#)]
34. Stegemeyer, H.; Behret, H. *Liquid Crystals*; Steinkopff: Heidelberg, Germany, 1994; Volume 2.
35. Conejo-Rodriguez, V.; Cuerva, C.; Schmidt, R.; Bardaji, M.; Espinet, P. Li⁺ and K⁺ ionic conductivity in ionic nematic liquid crystals based on 18-diaza-crown ether substituted with six decylalkoxy-*p*-cyanobiphenyl chains. *J. Mater. Chem. C* **2019**, *7*, 663–672. [[CrossRef](#)]



© 2019 by the authors. Licensee MDPI, Basel, Switzerland. This article is an open access article distributed under the terms and conditions of the Creative Commons Attribution (CC BY) license (<http://creativecommons.org/licenses/by/4.0/>).